

Account / Revue

# Microfluidics for kinetic inspection of phase diagrams

Jean-Baptiste Salmon, Jacques Leng\*

*Laboratoire du futur, unité mixte Rhodia/CNRS/Bordeaux-1, 178, avenue du Docteur Schweitzer, 33608 Pessac cedex, France*

Received 17 April 2008; accepted after revision 2 June 2008  
Available online 19 October 2008

## Abstract

We present a set of microfluidic tools developed for phase diagram studies. These tools are based, on the one hand on the formation of nanoliter-sized drops which undergo a complex thermal history, and on the other hand, on controlled evaporation used to concentrate a solution. We describe their use on crystallization from solution and we show that the small scale at which they work offers unprecedented control on the kinetic pathway followed in the experiments, and also helps to identify specific phase transitions that would be hidden in macroscopic conditions. *To cite this article: J.-B. Salmon, J. Leng, C. R. Chimie 12 (2009).* © 2008 Académie des sciences. Published by Elsevier Masson SAS. All rights reserved.

## Résumé

Nous présentons une gamme d'outils microfluidiques destinés à l'étude de diagrammes de phases. Ces outils sont basés sur deux techniques complémentaires: la formation de nano-gouttes et leur traitement thermique et l'évaporation contrôlée pour concentrer une solution à l'échelle du nanolitre. Nous décrivons la conception et l'utilisation de ces outils avec une attention particulière sur le contrôle qu'ils offrent sur l'exploration cinétique de diagrammes de phases de solutions aqueuses; en particulier, nous observons pour certains systèmes des états métastables qu'il serait difficile voire impossible d'observer à l'échelle macroscopique. *Pour citer cet article : J.-B. Salmon, J. Leng, C. R. Chimie 12 (2009).*

© 2008 Académie des sciences. Published by Elsevier Masson SAS. All rights reserved.

*keywords:* Microfluidics; Phase diagram; Kinetics

*Mots-clés :* Microfluidique ; Diagramme de phase ; Cinétique

## 1. Introduction

Phase diagrams represent an important basis for many industrial applications as well as academic studies. They are of special interest in many fields such as physical chemistry, biology, pharmacology, etc.

They cast a fundamental knowledge on equilibrium properties of the systems under study, and also help in understanding out-of-equilibrium features.

In soft matter for instance, they have been built extensively to describe the subtle physics of self-assembly of surfactant molecules in mixtures of oil and water for instance [1,2]. In that case, phase diagrams were obtained by traditional methods, that is, mixing in test tubes, and required a considerable work force both for preparation and for analysis. Another example lies in the

\* Corresponding author.

*E-mail addresses:* [jean-baptiste.salmon-exterieur@eu.rhodia.com](mailto:jean-baptiste.salmon-exterieur@eu.rhodia.com) (J.-B. Salmon), [jacques.leng-exterieur@eu.rhodia.com](mailto:jacques.leng-exterieur@eu.rhodia.com) (J. Leng).

realm of drug discovery, which makes an intensive use of high throughput screening methods and advanced tools, such as robotics, to investigate phase diagrams of medicinal molecules; crystallization conditions are tracked, and the occurrence of polymorphs and metastable states is of special interest as all forms of the same chemical do not exhibit an equivalent activity [3].

Microfluidics is a fairly recent technology that might contribute significantly to speed up such repetitive studies. Heir of microtechnologies, it offers the possibility of manipulating very small quantities of fluids — either gases or liquids — with ease and a neat control in the flow conditions [4,5]. It is a good candidate to decrease the amount of product used for studies, and is also promising in terms of *continuous screening*, as opposed to digital screening promoted by robotic assisted formulation.

Here, we present microfluidic tools we developed recently to study phase diagrams of (mostly aqueous) solutions at small scale. These tools offer interesting conditions and technological improvement to control and characterize the mixture of several compounds. However, before studying complex systems, we validate the microfluidic approach on *seemingly* simple systems, such as electrolytes in water, which actually display complex behaviors well evidenced by our devices.

More precisely, we highlight the good control of the *kinetic pathways* followed in the phase diagrams (Fig. 1) enhanced by the microfluidic format. With our devices, two routes are opened up with trajectories that are complementary: isoconcentration ( $T$ -jump at given concentration) or isothermal ( $c$ -jump at given temperature) (Fig. 1).

The first route uses the droplet technique [6,7] where small drops of solution are produced in oil and

act as individual reactors. The advantages are numerous: crystallization events are individualized and confined, the thermal control is good, etc. These drops undergo thermal trajectories that lead to the determination of the state of the solute, for instance crystallization.

The second technique integrates pervaporation for solvent removal. It is based on PDMS (polydimethylsiloxane, an elastomer commonly used for chip fabrication [8]) permeability and permits the concentration of a solution at the tip of a microchannel in a controlled manner [9,10]. It thus offers to raise the concentration and to scrutinize the phase diagram of aqueous solutions towards dense phases.

The two techniques are complementary, as illustrated in the schematic phase diagram of Fig. 1. They indeed allow the exploration of orthogonal planes in a complex phase diagram but also have specificities that we describe in detail in the rest of this paper. The drop technique is more versatile [4,11], permits to create and manipulate reactor-like microbatches at the nanoliter scale, with a very high throughput (up to  $10^3$  drops/s). This microfluidic approach offers numerous advantages as compared to other high throughput techniques (e.g. robotics) or batch studies — especially when dealing with thermal history — yet also suffers serious limitations that we list below. The evaporation technique delivers less throughput but is unique in the routes opened up in the exploration of a phase diagram [10,12]. As a matter of fact, it is one of the very few techniques that permits a controlled concentration of a solution whilst combining advantages of microfluidics (small amount of product, good thermal control, neat flow pattern at very low Reynolds number, etc.) and also allowing convenient analytical observations (microscopy, spectroscopy, scattering, etc.) against time and space directly in the microsystem.

The paper is thus organized into two parts concerning first the droplet technique and then the evaporation technique, with a special emphasis on the kinetic pathways made accessible. In particular, we show on a specific system (polymorphism of potassium nitrate) that the two approaches offer complementary views on the kinetic process of crystallization not accessible at a macroscopic scale.

## 2. The droplet technique: $T$ -jumps at the nanoliter scale

In this part, we describe a set of tools based on the formation of droplets subjected to a thermal history ( $T$ -jump and temperature cycles).

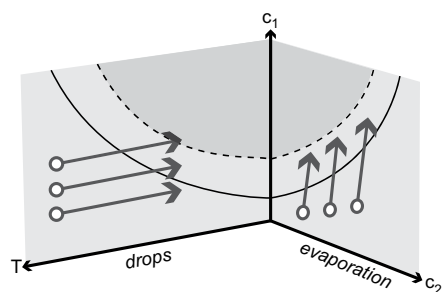


Fig. 1. Schematic phase diagram in the  $(c_1, c_2, T)$  plane where the  $c_i$ s are concentrations of solutes (in water most of the time) and  $T$  the temperature. The dark line typically sets the solubility limit between a fluid phase and a miscibility gap while the dashed line shows the limit of metastability. The arrows illustrate the routes followed in the two sets of microfluidic devices presented in this work: with the drop technique we explore a thermal route at constant composition while the evaporation technique increases concentration at constant temperature.

Some specific microfluidic geometries known as *hydrodynamic focusing* — where two streams of oil pinch a stream of water (Fig. 2) — are favorable to create drops of emulsion of controlled volume and velocity [13]. These drops have received considerable attention in the past 10 years. Indeed, each drop can be viewed as the equivalent of a batch reactor on the nanoliter scale and can be thus used for chemistry, synthesis, and screening operations such as crystallization conditions (especially for proteins [14]). We describe below such an use of drops for temperature induced crystallization.

Although fairly complex, the physics underlying the drop formation has been analyzed [15] and turns out to be a specific hydrodynamic regime of the two-phase flow of immiscible liquids, a consequence of a modified Taylor–Plateau instability where the confinement is of crucial importance. Once the drops are formed, the hydrodynamics within the drop is also difficult to quantify but both experimental [16] and numerical analyses [17] permit a fair description.

Hydrodynamic focusing may thus be seen as a manifestation of soft matter physics at the microscale where hydrodynamics is coupled to capillary effects and confinement. It permits the formation of droplets at a pace varying between 1 and  $10^3$  Hz typically, and of a volume in the range 0.1–100 nL. It is thus possible to

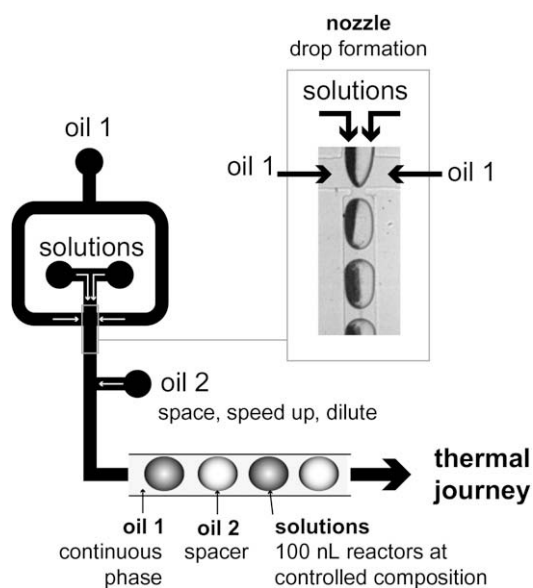


Fig. 2. Scheme of the droplet formation stage using the flow focusing technique in which the pinched droplet is composed of one or more components (aqueous solutions). A second inlet of oil (oil 2) permits either dilution with the same oil (as 1) or insertion of spacers made of an immiscible oil (e.g. fluorinated). The train of drops thus produced is sent to a thermal history, either flowing onto a thermal gradient or for storage and cycling temperature.

generate a very vast number of samples and this is why microfluidics is promising in terms of combinatorial chemistry [6].

In the context of nucleation studies, the best two things about small droplets are: (i) a well-defined volume  $V$ ; and (ii) separate crystallization events. It turns out to be of prime importance for controlling the stochastic event of nucleation *via* the nucleation frequency  $f = JV$  where  $J$  is the nucleation rate [18] (number of critical nuclei that occur per unit of time and volume). Additionally, the nucleation is mononuclear most of the time, that is, only one nucleation event per drop (which then exhausts the solution). The droplet technique has been devised actually a long time ago [19], but the technological improvement of flow control with microfluidics yields a much better control over the droplet volume and the temperature conditions. Indeed, we shall see below that it is possible to impose neat temperature conditions to the droplet and thus to analyze without ambiguity the kinetic events.

We give below a brief overview of the chip fabrication process (and flow and temperature control) and then describe their use for nucleation studies.

### 2.1. Overview of chips fabrication and control

Today, there are only a few ready-made microsystems available for sale. Instead, most microfluidic companies design for the clients' microsystems according to their needs. Each realization is costly. The common practice is thus to use homemade microsystems, which however requires some involvement in technological development. A clean room is ideal for fabrication but not compulsory for standard microfluidics; instead, a simple hood (equipped with a spin coater, hotplates, and an UV light) turns out to be sufficient to realize complex microfluidic systems.

Most of what we do is based on the recent development of microfabrication on hard and soft materials and the gamut of materials that can be processed is larger and larger [20]. Chips are designed and made at the laboratory. We start by designing a fluidic network on a specialized software and print it on a transparent slide (good resolution of typically 2500 dpi is required, e.g. pixel size of about 1  $\mu\text{m}$ ) and adequately obtained with offset printing. This slide serves as a mask to shine a photo-sensitive resist initially spincoated onto a silicon wafer. Where exposed, the resist chemically reacts to produce a hard product that does not dissolve in the subsequent development stage. This is the soft photolithography process that yields a wafer with patterns of given thickness, from 1 to 1000  $\mu\text{m}$ .

A silicon oil (PDMS + crosslinker) is poured onto the wafer, cured, and peeled off the wafer. Holes are punched out with a needle tip, and the PDMS slab is stuck onto a surface that seals it. The latter surface is made of glass most of the time to ensure transparency. However, thermal transfer is much better with silicon and we use this substrate for thermal treatment of droplets. In that case, we can produce either a gradient across the wafer by using two Peltier modules or impose a constant and homogeneous temperature ( $\pm 0.1$  °C) with a single Peltier module underneath the wafer; we can also cycle the temperature. In each case, we measure the temperature inside the channels by plugging temperature probes (thermocouple of  $\sim 100$   $\mu\text{m}$  of diameter) directly into the microsystem.

Flow control is achieved using syringe pumps; as the flow rates may be small, we noticed that some brands do not behave well and feature strong oscillations during the liquid distribution. In general, we use glass syringes (that can be warmed up with heating tape if required to ensure solubilization of a solute) and polymeric yet rigid (high Young modulus) tubing and connections in order to limit the transient behavior due to the overall elasticity of the system.

When relevant, we can choose to address a stream of liquid towards a particular channel, for storage or analysis for instance. This is made possible by using pinch valves that control the opening and closing of a tubing to which the corresponding channel is connected.

All the operations such as formulating, filling, addressing, temperature cycles, etc. are computer controlled *via* homemade programs in order to increase as much as possible automation, throughput, and reproducibility.

## 2.2. Crystallization in drops: scrutinizing a stochastic process

Based on the droplet technique, we derived several modes of manipulation that correspond to several needs or analysis. The three main modes are: (i) crystallization underflow which we describe below; (ii) droplet storage for temperature cycling; (iii) multicomponent chips for fast screening of crystallization conditions. We will show the advantages of microfluidics for these studies as well as some limitations when they occur.

### 2.2.1. On flight crystallization

Crystallization underflow is the most intuitive situation where a train of drops travels along a temperature gradient [21], say from hot to cold, which may induce the crystallization of a solute (Fig. 3, top). Counting

the number of crystals at a given position, that is, after a given time on the cool side, yields the nucleation frequency and further the nucleation rate. This strategy is interesting for rapid and on line screening as the composition of drops can be easily controlled and tuned to probe a large portion of a phase diagram. Note, however, that by measuring the nucleation rate we probe a *kinetic* feature of the system.

Here, one of the main advantages is really to produce a monodisperse emulsion, with therefore a *unique* volume  $V$ , and consequently a peaked nucleation frequency  $\propto JV$ . In particular, due to the small size of drops, the nucleation is *mononuclear* (only one nucleation event occurs per drop [22]) because the solution is exhausted immediately after any crystallization event, making the occurrence of another one unlikely. Note also that the drops are produced without surfactant molecules and it, therefore, limits the interferences between the potential nucleus and the surfaces. Finally, drops are independent of one another and a crystallization event does not induce another one in a neighboring one, as it may happen sometimes into concentrated emulsions [22].

Another interesting advantage of the microfluidic device is to impose strong and homogeneous supersaturations through the well-controlled temperature profile. Indeed, due to the silicon wafer, the temperature profile (which we measured [21]) is neat and drops undergo a  $T$ -jump in neat conditions. This is especially relevant when comparing the rapidity at which a macroscopic batch may change temperature.

We thoroughly used this experimental setup to study the nucleation of potassium nitrate ( $\text{KNO}_3$ ) crystals from aqueous solutions, a model system in the context of nucleation: it features a solubility that depends strongly on temperature and the solid does not wet the silicon oil we use to produce drops. We can thus safely study bulk nucleation.

We produce drops of soluble  $\text{KNO}_3$  at a frequency of about 1 Hz and drops flowing at a velocity of  $\sim 4$  mm/s towards a cold zone. We varied the ramp with an initial temperature of 60 °C followed by a steep ramp reaching a plateau value ranging in  $T_f = 5\text{--}20$  °C. The entrance of the cold zone is ascribed to  $t = 0$  and we monitor the drops farther on in the chip with the equivalence time/distance offered by a well-controlled flow rate. In this device, we reach relatively high supersaturations (relative excess of concentration above to the solubility), of the order of 10, which are not accessible in bulk reactors; this is due to the high cooling rate along with the small size of the drop reactors.

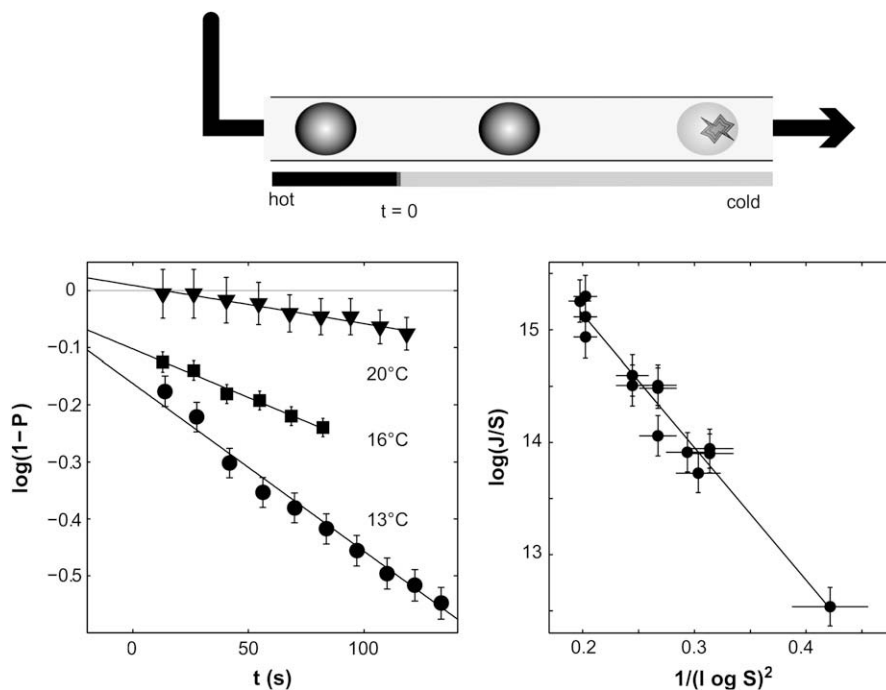


Fig. 3. On flight crystallization: drops of solution are produced at high temperature and then flow in a cold environment. By monitoring the droplets that contain a crystal against distance from the beginning of the cold zone, we extract (a) the probability  $P$  for having a crystal against time and (b) a nucleation rate  $J$  against supersaturation  $S$ .

We number the crystals against position to extract a probability  $P$  of having one crystalline germ after a given time; we observe that temperature of the cold place strongly influences  $P$  (Fig. 3) and that this probability increases with time: the longer we wait, the more likely to have a seed. For a stochastic process such as mononuclear nucleation  $P(t) = 1 - \exp(-Jt)$  [18,23,24] and we can extract  $J$ , the nucleation rate, from our measurements.

This rate is an important kinetic characterization of the solute; it can be used as such for production purposes, or serves as a basis for a better understanding of the nucleation process. The most basic view of the process is depicted by the classical theory of nucleation [18,22]. It states a link between the supersaturation  $S$  of the solution and the nucleation rate such as  $J \approx AS \exp[-B/(\log S)^2]$ . The agreement with our data is indeed good (Fig. 3) and the key parameter we can then extract from this comparison is the surface tension between the critical nucleus and mother liquor: we found  $\gamma = 19 \pm 1$  mN/m, in close agreement with previously published results [19]. Additionally, the prefactor  $A$  gives a strong indication that the nucleation is heterogeneous, and we did confirm this with complementary experiments (see later on in the text). Note that the

classical theory of nucleation is certainly too simple for electrolyte crystallization but is, nevertheless, a good basis for comparison with the literature data.

The interest of our platform is quite obvious here: statistics can be improved by waiting for a larger number of drops; we found that typically 200 drops are enough for having good results although it is straightforward to wait longer if needed. However, the setup suffers from limitations. The first one is intrinsic to nucleation: when we reproduced several times the previous *on flight* crystallization experiment with the same batch of potassium nitrate, we found a fairly strong deviation from the  $\gamma$  presented before. When averaging over many sets of data, we find  $\gamma = 21 \pm 5$  mN/m. Below, we impute this effect to heterogeneous nucleation on impurities coupled to the small size of the system and suggest that we never probe twice the same selection of impurities.

The second limitation is due to the design of the chip: the given velocity of the drops ( $\approx$  mm/s) and the total length  $L$  of the system ( $\approx$  10 cm) define a maximum time that we can probe ( $\approx$  a few hundreds of seconds) and thus limits the nucleation frequency we can measure. It, therefore, precludes studies of slow nucleation such as that of protein crystals.

Finally, we also note solvent issues: the use of organic solvents is a major difficulty essentially for the formation of drops. It, therefore, sets a strong limit as to the conditions we can study.

### 2.2.2. A chip for rapid solubility measurements

At least one of the previous limitations can be easily solved: in order to study slow nucleation, we can stop the flow and store the droplets, and wait long enough to observe crystallization. Doing so, we developed a series of chips based on droplet storage for nucleation studies. The first we present is devoted to fast solubility screening.

Solubility is a thermodynamic measurement (as opposed to the nucleation rate which is of a kinetic nature) and one way to measure it is to go from the crystallized towards the dissolved solute. The temperature and concentration at which it occurs define the solubility conditions.

For a fast screening of solubility conditions, we worked out a fully automated chip where a set of parallel channels are addressable individually and are filled with trains of drops at a given composition (Fig. 4A). Once one channel is filled, we switch to the next one with the set of pinchable valves that make the channels addressable, wait long enough to ensure equilibration of the new composition, and fill the following channel, etc. This operation is fully automated, takes about 20 min for a consumption of about 250  $\mu\text{L}$  of concentrated solution [25]. We first cool down the device to induce crystallization in all the droplets and then apply a temperature gradient across the microsystem parallel to the channels (Fig. 4A) in order to establish a gradient in a complementary direction of the phase diagram.

Doing so, we observe crystals in a specific portion of the plane ( $c$ ,  $T$ ) which permits a clear identification of the ( $c$ ,  $T$ ) conditions for which crystals do dissolve into drops, that is, solubility conditions. We used it to measure the solubility of potassium nitrate and adipic acid [25] in water, and found an excellent agreement with the literature data.

### 2.2.3. Probing polymorphism and heterogeneous nucleation

We developed a device devoted to the study of slow nucleation kinetics and which also yields improved statistics. Indeed, long term incubation is problematic in PDMS devices due to drop coalescence and evaporation. Drops are formed without surfactant molecules and they tend to coalesce with time (note that Ostwald ripening is much limited due to the very narrow size

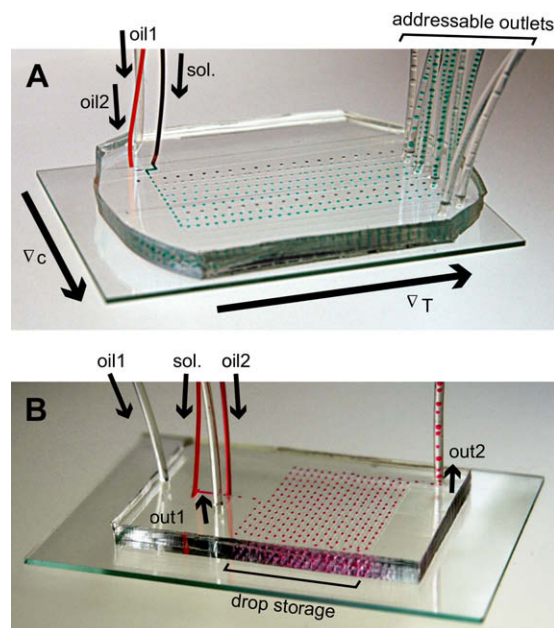


Fig. 4. (A) Device for fast solubility screening. The droplets are formed at a given composition and addressed towards a particular channel with the use of pinchable outlets. Each channel is filled with a train of drops at a given composition and the composition is changed from channel to channel in order to establish a gradient of composition. Once filling is achieved, a temperature gradient is imposed to the chip. It yields a direct reading of the crystallization conditions in the plane ( $c$ ,  $T$ ). (B) A device for storage of typically 300 drops: the PDMS microfluidic chip is sealed here on a glass slide for illustration purpose. For the real application of thermal cycling, we used a device contacted with a silicon substrate stuck onto a Peltier module that regulates temperature.

distribution of the drops). To prevent coalescence, we use spacers of fluorinated oil. However, long term storage in PDMS devices remains limited due to unavoidable evaporation (see next part) and glass devices for instance must be fabricated to prevent this effect.

The device we developed consists of a droplet generator connected to a serpentine in which hundreds of drops can be stored (Fig. 4B). The device is in contact with a silicon wafer so to apply neat temperature cycles. We recover the advantages of small drop manipulations and add new features. Besides, we can monitor directly inside the (standing still) droplets what habits the crystals follow, wait long enough to see whether the observed forms are stable, temperature cycle the cell many times to obtain reproducibility information on nucleation, etc.

Doing so, we observed actually that all droplets do not systematically behave the same way. In the case of aqueous solutions of  $\text{KNO}_3$ , we could track the

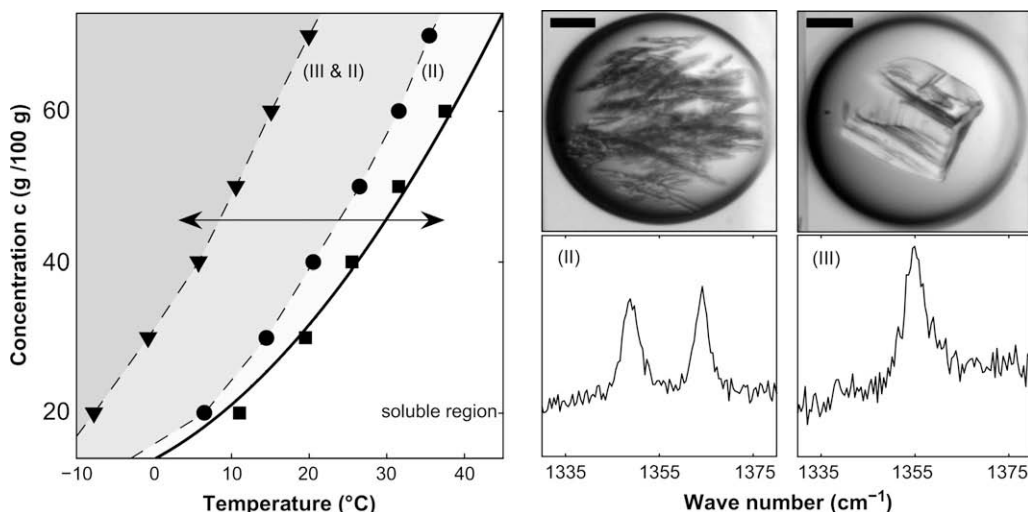


Fig. 5. Evidencing polymorphs of potassium nitrate crystallized from aqueous solutions by the habit and the Raman spectroscopic signature (right; the bar represents 100  $\mu\text{m}$ ). The two polymorphs have different solubilities (left). The solid line represents literature data while symbols correspond to the solubility limits (squares and circles) and limit of metastability (triangles) measured with the device. (II and III refer to the conventional naming [26,27] of the stable and metastable forms of  $\text{KNO}_3$ , respectively. Dashed lines are guides for the eye.)

occurrence of several polymorphs, and even measure the solubility limit of the various polymorphs. To do so, we just cooled down the hundreds of droplets and warmed them up until total dissolution of the crystals; we witnessed the existence of two families of crystals that dissolve at different temperatures. A more detailed observation reveals (Fig. 5) that the two families actually also have specific crystallization habits and feature different vibrational responses as probed by Raman microspectroscopy. Carrying up the dissolution experiments systematically with drops prepared at several compositions, we were able to measure two solubility curves [28].

These measurements are made possible because nucleation events are individualized: they are independent of one another as occurring in different droplets. In a traditional batch, the nucleation is often polynuclear making difficult the discrimination between several species. There are also polymorphic transitions during which the metastable phase disappears for the most stable one [29].

Additionally, it is possible to track the nucleation kinetics in detail and measure the nucleation rate of crystallisation over a much longer period of time (minutes to hours) than for flowing drops. We find that the nucleation is heterogeneous and governed by impurities in the solvent. With the good statistics we access, we observe that the probability of having crystals in a drop is *not* a single exponential at long times as expected from homogeneous nucleation

theory. It suggests heterogeneous nucleation, and we showed actually that it is possible to evidence a *distribution of impurities* which activate nucleation over a large degree of supersaturation, making the definition of a single nucleation rate rather awkward, if not totally impossible. Instead, we could measure a distribution of nucleation rates and assess the existence of different impurities [30]. Here again, the small size of the microbatches helps to select different impurities as each drop contains a much smaller number of impurities than a conventional batch.

### 3. Concentration pathway: evaporation-based microsystems

We now turn to the second category of microfluidic devices we developed and which is based on evaporation. Evaporation is a common means to extract solvent from a solution and to concentrate it: it thus helps exploring a phase diagram at constant temperature<sup>1</sup> towards high concentrations. Here, we use evaporation on the microscale to bring unprecedented control of the kinetic trajectory in the phase diagram. We present the device at work, what sort of exploration it makes possible, and will eventually conclude by highlighting the complementarity with the drop technique.

<sup>1</sup> Put aside heat flow due to evaporation and which is readily absorbed into the bulky system, a real advantage of microsystems making them quasi-isothermal.

### 3.1. Linear evaporator: principle

#### 3.1.1. Evaporation induced flow

The microevaporator is based on pervaporation across an integrated PDMS membrane to remove solvent from a solution [31]. The device is made by a superimposition of several PDMS layers (Fig. 6) that carry liquid and gas, respectively. The layers are separated by a thin membrane ( $e \sim 10 \mu\text{m}$ ) through which solvent (mostly water in our case) permeates and evaporates. The vapor is driven away by a gas flux that ensures a reproducible boundary condition.

We define a volume flux of evaporation which is homogeneous to a velocity when normalized by the membrane exchange area: this is the evaporation velocity  $v_e$  of the order of 1–50 nm/s [10] — which depends on sorption of water in PDMS [31] — a key parameter for controlling the process. From  $v_e$ , we also define an evaporation time  $t_e = h/v_e$  with  $h$  the height of the channel (Fig. 6). This time represents the time needed to empty one channel volume ( $t_e = 100\text{--}1000$  s).

The water lost by evaporation is replenished by a flow induced from the reservoir. Solving the Stokes equation (Reynolds number is small) with a sink term on the membrane as a boundary condition readily gives the  $z$ -averaged mean velocity induced by evaporation:  $\langle v(x) \rangle_z = -x/t_e$  which reaches, at the end of the

evaporator,  $v_0 = -L_0/t_e$ . We find here a simple linear link between the mean entrance velocity  $v_0$  and the evaporator linear size  $L_0$  [9,10,32], and this is a very good approximation although we observe experimentally that the induced velocity does not quite drop to 0 when  $x \rightarrow 0$  due to edge effects.

The integrated pervaporation offers a dynamic control over evaporation conditions and induced flow. Indeed, if we flow a humid gas in the evaporation compartment (gas channel, Fig. 6), or even water, evaporation is slowed down or even stopped as compared to a dry gas. The time it takes for the induced flow field to feel the change of conditions is essentially limited by diffusion across the PDMS membrane, of order of  $D_w/e^2 \sim s$  (where  $D_w$  is the diffusion coefficient of water in PDMS,  $\sim 10^{-9} \text{ m}^2/\text{s}$ ). It is thus possible to readily tune the evaporation and thus the induced flow, in a matter of seconds [10], and it offers interesting possibilities for phase diagram studies as we will show below.

#### 3.1.2. Concentration of a solute

Due to the induced flow, the device enables concentration of a solute: indeed, the incoming velocity  $v_0$  — of order of 10–100  $\mu\text{m}/\text{s}$  — brings up fresh solute at a flux  $j_0 = c_0 v_0 = c_0 L_0/t_e$  into the evaporator as long as the solute is at  $c_0$  concentration in the reservoir (Fig. 6). The device is, therefore, continuously fed by solution; the solute is driven by the flow towards the tip of the capillary where it accumulates, and diffuses back. It follows a diffusion–advection dynamics from which we can derive the concentration field [10].

We do not give details here but simply the main ingredients. We identify a typical size  $p$  where the advection flux  $j_A \sim -cp/t_e$  is equivalent to that of diffusion  $j_D \sim -Dc/p$  with  $c$  the local concentration and  $D$  the diffusion coefficient of the solute. Thus  $p \sim \sqrt{Dt_e}$  defines the spatial extent onto which solute accumulates. The exact shape of the profile is Gaussian and can be understood by analogy with sedimentation. In the latter case, a homogeneous body force acts onto the solute and induces an exponential concentration profile. In microevaporation, the force increases linearly with distance from the tip and the concentration decay is amplified, and scales like  $\exp(-x^2/2p^2)$  [10].

The sketch of Fig. 6 (bottom) summarizes the physics at work: the concentration rate of solute is essentially determined by the knowledge of: (i) the evaporation time of the device ( $t_e = h/v_e$ , calibrated elsewhere); and (ii) the diffusion of the solute  $D$ . From

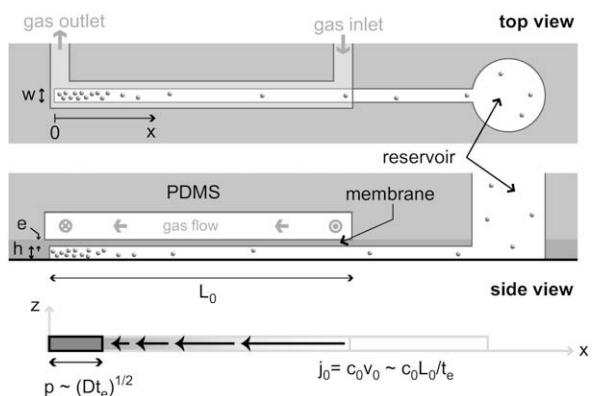


Fig. 6. Sketch of the linear evaporator geometry: top and side views showing the gas and liquid layers and the thin PDMS membrane in between (typical dimensions:  $e \sim 10 \mu\text{m}$ ,  $h \sim 20 \mu\text{m}$ ,  $w \sim 200 \mu\text{m}$ ,  $L_0 \sim 10 \text{ mm}$ ). Bottom: sketch of the main control parameters: the evaporator behaves as a linear pump that delivers a flux  $j_0 = c_0 v_0 = c_0 L_0/t_e$  where  $c_0$  is the concentration inside the reservoir,  $v_0$  the entrance velocity, and  $t_e$  the evaporation time (see text for details). Due to the advection–diffusion dynamics, the solute accumulates at the tip of the device on a scale  $p \sim \sqrt{Dt_e}$ . As the solute flux  $j_0$  is conserved, the concentration enrichment rate in the  $p$ -box is well-defined and scales like  $\dot{c} \sim j_0/p$ .

$t_e$  (or  $v_e$ ) we deduce the velocity field [ $v(x) = -x/t_e$ ] which is then used to know the solute feeding flux  $j_0 = c_0 v_0$ ; this solute is driven by advection, slows down around the tip of the capillary where it accumulates. With the diffusion coefficient we build the size  $p$  where the solute accumulates  $p \sim \sqrt{D t_e}$  and the accumulation rate is then simply obtained by solute conservation: the flux  $j_0$  is conserved (no loss of solute in the device) and feeds the  $p$  zone:  $dc/dt = c_0 L_0 / p t_e$ .

This simplified description actually works well [10,12]. Yet, it is based on the knowledge of the induced velocity field, supposed here linear and steady, but which is in reality coupled to the concentration (and thus time dependent). As a matter of fact, evaporation depends on the chemical potential difference across the membrane, which varies with the actual concentration. However, for dilute solution we may safely assume it does not alter the previous picture (and we checked it is the case) and the scaling laws are useful guides for planning an experiment.

### 3.2. Electrolyte nucleation: simple phase diagrams

Of prime interest is the ability of microevaporators to concentrate a solution in a well-controlled manner. We used ideal solutions (fluorescein in water at a concentration below  $10^{-3}$  M) to check that the quantitative agreement between theory and experiments [10]. With the electrolyte nucleation, we go a step further as the system is not ideal anymore. Yet, we observed that our model is a fair guide to understand the kinetics at work.

#### 3.2.1. Simple nucleation

The linear evaporator thus offers to concentrate a solute in a localized zone. The evaporation velocity and the solute mobility cast an accumulation size  $p$ , which is enriched at a pace  $\dot{c} = c_0 L_0 / p t_e$ . The two main control parameters are  $c_0$  the concentration in the reservoir and  $L_0$  the length of the evaporator.

We used them to check out the prediction of previous paragraph with a simple system: potassium chloride (KCl). This electrolyte is interesting as it presents a well-defined solubility (with a small metastability extent [33]) nearly independent of the temperature and a diffusion coefficient  $D$  nearly independent of the concentration even at high concentration. When injected into a microevaporator, we observe that a given time  $t_c$  is needed to induce a nucleus. This time depends both on  $c_0$  and  $L_0$  and scales linearly with  $c_0 L_0$  (Fig. 7), as expected from theory. Note that we do not measure the solubility but the metastability limit instead.

Also promising for controlled  $c_0 L_0$  in confined geometry, we observe that nucleation is followed by growth at a controlled pace. We measured systematically the velocity at which the crystals grow and the growth rate also scales with  $c_0 L_0$ , at least during the early stage (Fig. 7), showing that the control on growth is also cast by the geometry. From the growth experiments, the scaling of the growth rate with  $c_0 L_0$ , and simple arguments of solute conservation [10,12] we also measure the density of the growing phase, here that of the crystal, in good agreement with the literature data. The microevaporator thus yields kinetic and thermodynamic data.

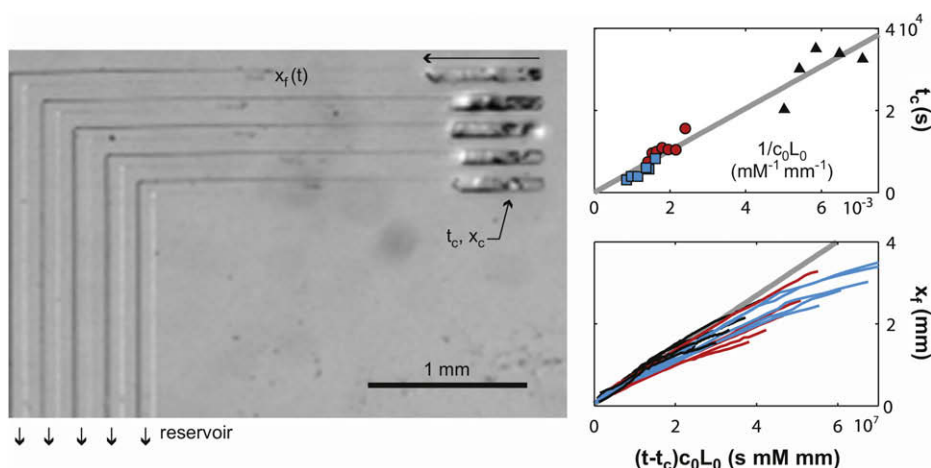


Fig. 7. Analysis of KCl nucleation and growth. (Top) Picture of five linear evaporators having different lengths (hence different concentration rates) and which are connected to the same reservoir at  $c_0$ . (Bottom) Analysis of the induction time for crystallization ( $t_c$ ) and growth dynamics after nucleation against time and reduced time (see text).

### 3.2.2. Polymorphic nucleation

The microevaporation device is complementary to the drop technique as the former is used to enrich the concentration at the tip of a capillary at constant temperature while this is the opposite for the latter. This complementary is well demonstrated when studying the nucleation of  $\text{KNO}_3$ . With the drop technique we could observe two families of crystals having different crystallization habits and solubilities (Fig. 5).

For potassium nitrate in water (Fig. 8), we observe in a microevaporation channel the formation of a faceted crystal after some induction time. After a certain time, however, the crystal spontaneously transforms into another one with a different habit; it seems that the faceted crystal breaks down into pieces with round shapes. We used space and time resolved Raman microspectroscopy to monitor the vibration of the nitrate bound in solubilized and crystalline forms, and observed that the main vibration mode, around  $1050\text{--}1060\text{ cm}^{-1}$  indeed shifts upon transition; it thus proves that the structure of the crystal changes and we could assess the nature of the crystals from the vibrational analysis [26]. The transition is very swift ( $\sim\text{ms}$ ) and corresponds to a polymorphic transition that decreases the free energy of the system: the first crystal is not the most stable one yet is selected probably because of a higher nucleation rate. Strong curvature at the level of the facets is likely to cause the transition. In a future work, we plan to study systematically the

transition by multiplying the number of tests on a chip and measuring for instance the lifetime of phase III.

The case of microevaporators is quite analogous to that of drops: the size of the reactor is small,  $\sim\text{nL}$ , however, supersaturation is moderate. Once a nucleation event occurs, it exhausts the solution and it is very unlikely that another one takes place. In accordance to Ostwald's step rule [29], the metastable phase (state III) appears first and is followed by a transition from state III to state II.

### 3.3. Complex phase diagram

The most promising feature of the microevaporation technique is that it offers the possibility of manipulating virtually any solute in water, from ions to colloids. Starting from a dilute solution, the latter is concentrated and only patience can limit the duration of an experiment. It implies that there is no complication about the manipulation of viscoelastic fluids, and also that even a poorly soluble solute can be studied. It is also possible to study complex fluids where the droplet technique would fail because of intrinsic limitations (non-linear rheology, capillary effects, wetting, etc.).

We analyzed the accumulation behavior of a poorly soluble surfactant molecule: docusate sodium salt (AOT) in water at room temperature. With this molecule whose phase diagram is well known [34], we observed a sequence of kinetic events [12] that

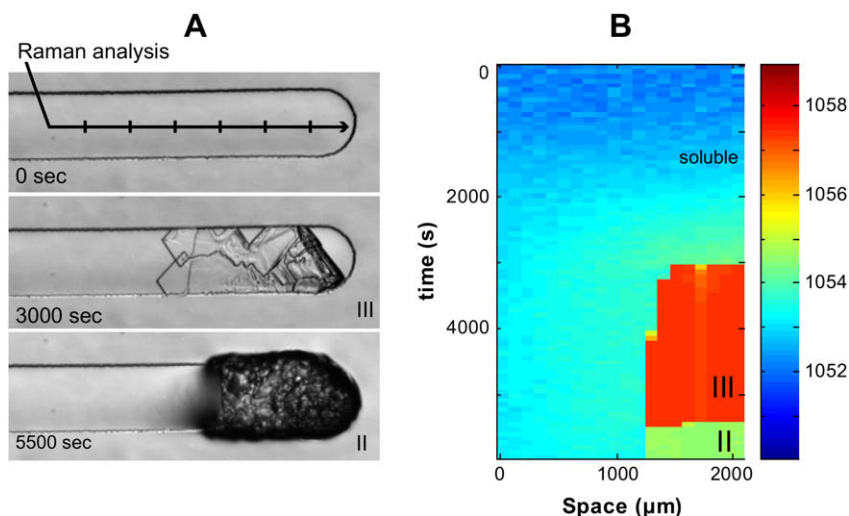


Fig. 8. (A) Polymorphic transition of  $\text{KNO}_3$  between the metastable form (III) which appears first and the stable one (II). The transition occurs within seconds and manifests itself by crystal habit changes (the width of the channel is  $200\text{ }\mu\text{m}$ ) and (B) by a specific signature in the vibrational modes as probed by Raman confocal microspectroscopy. The color bar represents the frequency range (units of  $\text{cm}^{-1}$ ) of vibrations probed in the microchannel of the solution and solid, and for which the intensity is plotted.

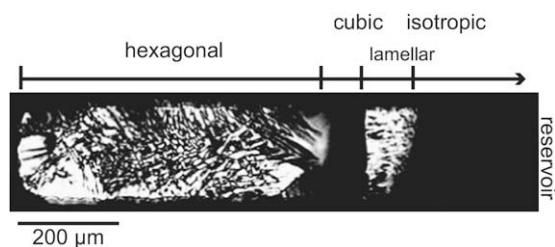


Fig. 9. Probing the accumulation behavior of a poorly soluble surfactant molecule (AOT) in water. Observation at a late stage in between crossed polarizers showing a sequence of phases that can be identified from their textures.

eventually leads to the growth of a dense phase in the microcapillaries. Observed in between crossed polarizers (Fig. 9), the capillary turns out to be filled with a structure made of bands that display specific birefringent properties. These textures correspond to different organizations of the molecules within mesophases. It is, therefore, possible in a single experiment to obtain a qualitative view of the phase diagram, assuming we are able to identify the phases from their textures.

Moreover, the pace at which the dense phase grows is *strictly* proportional to  $c_0L_0$  [12] which shows that the geometry leads to a good control of growth rate and that we can extract an estimate of the dense phase density. We obtain a value that corresponds to the concentration of the densest phase in the diagram (hexagonal phase) and we also monitor that this phase somehow ripens with time during the growth, suggesting that it gets more and more compressed, up to potentially 100% of surfactant.

This results opens up fascinating questions as to the mass transfer from a dilute solution up to a very dense phase in surfactant systems: we wonder what fixes the width of the bands in the capillary of Fig. 9 and how to describe the interplay between compressibility and mobility for the successive mesophases. The soft

matter physics at work is complex but promises a fair characterization of the band structure of Fig. 9, which is required to obtain information of the underlying phase diagram from the kinetic observation.

### 3.4. Dynamic phase diagram exploration

We conclude the description of microevaporation by a selection of kinetic pathways accessible in a phase diagram *via* this technique. We represent in Fig. 10 the several pathways microevaporation makes possible in the phase diagram of a two-component system in water, say:

- *continuous quench*: it is the experiment we presented before. The tip of a capillary is enriched at a constant rate that is tunable with control parameters such as  $c_0, L_0$ ;
- *dynamic quench*: we also mentioned it; by changing evaporation conditions (and thus the chemical potential gradient across the membrane), it is possible to go back and forth around a point of interest;
- *sequences*: made possible when working with open access reservoirs, where the solution can be changed by pipetting a new one, and which permits to explore orthogonal directions in the phase diagram (enriching say a protein solution, and then a salt solution, etc.) It is also possible to wait at a given point of the phase diagram by injecting pure water in the reservoir.

The various routes described before are especially important to bring up control in the kinetics of phase diagram inspection. For instance, when attempting to crystallize proteins, it is well known that a high supersaturation is required to induce the formation of many nuclei [11]; the subsequent stage of desaturation – induced by flowing a humid gas – reduces the number of crystals and permits the neat growth of a few of them.

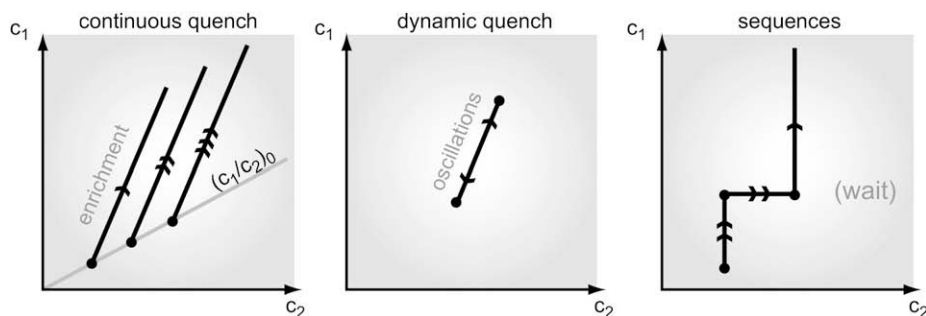


Fig. 10. Kinetic pathway in a two-component in water phase diagram that microevaporation makes possible to explore.

It results in principle in very few crystals of large size adequate for X-ray scattering.

Additionally, the microevaporation environment is virtually gravity-free, and definitively free of spurious turbulent effects. We, therefore, expect neat conditions for growing good quality protein crystals, and also and particularly studying the influence of kinetics in the occurrence of various polymorphs and out-of-equilibrium structures such as gels and clusters [35].

#### 4. Conclusion

We presented a set of microfluidic tools that we develop with the aim of acquiring fine control of the kinetics in phase diagram studies. These tools are based on the one hand on the formation of nanoliter-sized drops which undergo a complex thermal history. Each drop is a tiny reactor in which single events such as crystallization may occur. It yields a range of advantages over traditional techniques for studying nucleation from a solution. In particular, we can observe individualized crystallization events that do not influence each other. This is particularly interesting when metastable phases occur, that would readily disappear in a macroscopic batch. On the other hand, we developed tools that work at constant temperature and induce the concentration of virtually any solution in a nanoliter-sized test tube. We showed on polymorphism in potassium nitrate that the two sets of tools are complementary, yet possess their own specificities. These tools are now well characterized and fully automated and operational. We plan to use them in a future work for systems that are prone to out-of-equilibrium effects such as proteins and colloids and to reach with confidence the complex world of soft matter systems. This cannot be fully achieved without a deeper theoretical understanding of the many phenomena that couple equilibrium to kinetics, which profoundly alter the simplest approach we presented here and also may generate unique states of matter.

#### Acknowledgements

We are grateful to M. Joanicot and also thank colleagues who contributed to this work: A. Ajdari, G. Cristobal, A. Crombez, P. Guillot, P. Laval, P. Moreau. We also thank *Rhodia* and *Région Aquitaine* for funding and support.

#### References

- [1] P.G. de Gennes, C. Taupin, *J. Phys. Chem.* 86 (1982) 2294.
- [2] D. Roux, A.M. Bellocq, *Phys. Rev. Lett.* 52 (1984) 1895.
- [3] S. Veessler, F. Puel, G. Fevotte, *STP Pharm. Prat.* 13 (2003) 1.
- [4] H.A. Stone, A.D. Stroock, A. Ajdari, *Annu. Rev. Fluid Mech.* 36 (2004) 381.
- [5] T.M. Squires, S.R. Quake, *Rev. Mod. Phys.* 77 (2005) 977.
- [6] M. Joanicot, A. Ajdari, *Science* 309 (2005) 887.
- [7] H. Song, D.L. Chen, R.F. Ismagilov, *Angew. Chem., Int. Ed.* 45 (2006) 7336.
- [8] J.C. McDonald, G.M. Whitesides, *Acc. Chem. Res.* 35 (2002) 491.
- [9] G.C. Randall, P.S. Doyle, *Proc. Natl. Acad. Sci. U.S.A.* 102 (2005) 10813.
- [10] J. Leng, B. Lonetti, P. Tabeling, M. Joanicot, A. Ajdari, *Phys. Rev. Lett.* 96 (2006) 084503.
- [11] B. Zheng, J.D. Tice, L.S. Roach, R.F. Ismagilov, *Angew. Chem., Int. Ed.* 43 (2004) 2508.
- [12] J. Leng, M. Joanicot, A. Ajdari, *Langmuir* 23 (2007) 2315.
- [13] S.L. Anna, N. Bontoux, H.A. Stone, *Appl. Phys. Lett.* 82 (2003) 364.
- [14] B. Zheng, C.J. Gerdt, R.F. Ismagilov, *Curr. Opin. Struct. Biol.* 15 (2005) 548.
- [15] P. Guillot, A. Colin, A.S. Utada, A. Ajdari, *Phys. Rev. Lett.* 99 (2007) 104502.
- [16] G. Cristobal, L. Arbouet, F. Sarrazin, D. Talaga, J.-L. Bruneel, M. Joanicot, L. Servant, *Lab Chip* 6 (2006) 1140.
- [17] F. Sarrazin, T. Bonometti, L. Prat, C. Gourdon, *J. Magnaudet, Microfluid Nanofluidics* (2007).
- [18] D. Kashchiev, G.M. van Rosmalen, *Cryst. Res. Technol.* 38 (2003) 555.
- [19] M.L. White, A.A. Frost, *J. Colloid Sci.* 14 (1959).
- [20] H. Becker, L.E. Locascio, *Talanta* 56 (2002) 267.
- [21] P. Laval, J.B. Salmon, M. Joanicot, *J. Cryst. Growth* 303 (2007) 622.
- [22] G.M. Pound, *Ind. Eng. Chem.* 44 (1952) 1278.
- [23] D. Turnbull, J.C. Fisher, *J. Chem. Phys.* 17 (1949) 71.
- [24] J.C. Fisher, *J. Chem. Phys.* (1949) 429.
- [25] P. Laval, N. Lisai, J.B. Salmon, M. Joanicot, *Lab Chip* 7 (2007) 829.
- [26] M.H. Brooker, *J. Phys. Chem. Solids* 39 (1978) 657.
- [27] D.M. Adams, P.D. Hatton, A.E. Heath, D.R. Russel, *J. Phys. C: Solid State Phys.* 21 (1988) 505.
- [28] P. Laval, C. Giroux, J. Leng, J.B. Salmon, *J. Cryst. Growth* (2008). doi:10.1016/j.jcrysgro.2008.03.009.
- [29] P.R. ten Wolde, D. Frenkel, *Phys. Chem. Chem. Phys.* 1 (1999) 2191.
- [30] G.M. Pound, V.K. La Mer, *J. Am. Chem. Soc.* 74 (1952) 2323.
- [31] E. Favre, P. Schaetzel, Q.T. Nguyen, R. Clement, J. Neel, *J. Memb. Sci.* 92 (1994) 169.
- [32] E. Verneuil, A. Buguin, P. Silberzan, *Europhys. Lett.* 68 (2004) 412.
- [33] D.S. Coleman, P.D.A. Lacy, *Mater. Res. Bull.* 2 (1967) 935.
- [34] J. Rogers, P.A. Winsor, *J. Colloid Interface Sci.* 30 (1969) 500.
- [35] A. Stradner, H. Sedgwick, F. Cardinaux, W.C. Poon, S.U. Egelhaaf, P. Schurtenberger, *Nature* 432 (2004) 492.